ELECTRONIC SUPPLEMENTARY INFORMATION

Probing halogen-halogen interactions in solution

Virgile Ayzac, Matthieu Raynal, Benjamin Isare, Julien Idé, Patrick Brocorens, Roberto Lazzaroni, Thibaud Etienne, Antonio Monari, Xavier Assfeld, Laurent Bouteiller

Techniques.

Small-angle neutron scattering (SANS). Small-angle neutron scattering measurements were made at the LLB (Saclay, France) on the Pace and PA20 instruments, at two distance-wavelength combinations to cover the 4.1 10^{-3} to 0.23 $Å^{-1}$ q-range, where the scattering vector q is defined as usual, assuming elastic scattering ($q=(4\pi/\lambda)\sin(\theta/2)$, where θ is the angle between incident and scattered beam). Data were corrected for the empty cell signal and the solute and solvent incoherent background. A light water standard was used to normalize the scattered intensities to cm^{-1} units. The data was fitted with the form factor of a long rigid cylinder with a circular cross-section and a homogeneous contrast according to reference 1 or with the DANSE software SasView.

Differential scanning calorimetry (DSC). Solution-phase differential scanning calorimetry measurements were performed on a high sensitivity TA Instruments nDSC III system (baseline noise ± 15 nW). The sample cell (0.3mL) was filled with the bisurea solution and the reference cell with the corresponding solvent. The capillary cells were not capped, and a constant pressure of 5 10^5 Pa was applied. The solutions were analyzed using at least 3 full heating/cooling cycles, at 1 °C min^{-1}. The transition temperature, T**, was measured from the second heating scan.

Fourier transform infrared (FTIR) spectroscopy. Solution spectra were measured on a Nicolet iS10 spectrometer in KBr cells of 1.0 mm pathlength and are corrected for air, solvent and cell absorption. The temperature was controlled with a digital temperature controller (West 6100+) from Specac.

Circular dichroism (CD) spectroscopy. CD measurements were performed on a Jasco J-1500 spectrometer equipped with a Peltier thermostated cell holder and Xe laser (lamp XBO 150W/4). Data were recorded with the following parameters: 20 $nm.min^{-1}$ sweep rate, 0.05 nm data pitch, 2.0 nm bandwidth, and between 300 and 220 nm. Solvent and cell contributions at the same temperature were subtracted from the obtained signals. 1-chlorodecane was selected as solvent instead of 1-chlorohexane because of its reduced absorption in the region of interest. A 1 mm closed quartz cell was used. For CD analyses performed at 90°C, the solution was heated to 90°C (1°C.min^{-1}) and kept at this temperature for 15 minutes before recording the spectrum. Molar CD values are reported in $L.mol^{-1}.cm^{-1}$ and are expressed as follows: $\Delta\varepsilon=\theta/(32980\times l\times c)$ where θ is the measured ellipticity (mdeg), l is the optical pathlength in cm, and c is the concentration in $mol.L^{-1}$. For all samples, LD contribution was negligible ($\Delta LD < 0.005$ dOD) and the shape of the CD signal was independent of the orientation of the quartz slide.

Additional experimental data.

Table S1. Solubility data for bisureas at 10 mM and room temperature in various solvents (S = fluid solution, G = transparent and viscoelastic solution, I = insoluble).

	cyclohexane	propylbenzene	toluene	benzene	1-bromohexane	1-chlorohexane	diethyl ether	ethyl acetate	dichloromethane	tetrahydrofuran
H	G	G	G	G	G	G	I	I	S	S
B	I	G	G	I	G	G	I	I	S	S
C	I		G		G	G	I	I	S	S

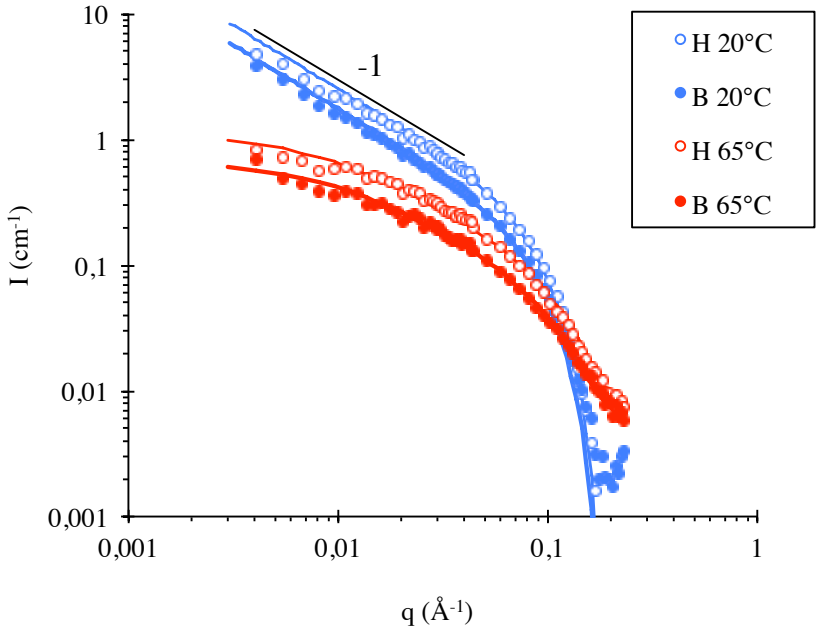

Figure S1. SANS intensity versus scattering vector for solutions of bisurea **B** or **H** in D_8-toluene (0.6 wt%, ca 5 mM). The curves are fits according to a model for long rigid cylinders with a circular cross-section and a homogeneous contrast (see parameter values in Table S2).

Table S2. Parameter values deduced from the fit of the SANS data (Figure S1) according to a model for long rigid cylinders with a circular cross-section and a homogeneous contrast.

bisurea	temperature (°C)	ρ [a] ($Å^{-2}$)	L [b] (Å)	R [c] (Å)	n_L [d] ($Å^{-1}$)
B	20	$1.26\ 10^{-6}$	> 300	21.2	0.48
	65		100	16.9	0.18
C	20	$1.39\ 10^{-6}$	> 300	18.9	0.47
	66		95	16.7	0.18
H	20	$0.94\ 10^{-6}$	270	20.9	0.48
	65		110	15.4	0.19

[a] scattering length densities (calculated from the atomic bound coherent scattering lengths). $\rho_{toluene} = 5.66\ 10^{-6}\ Å^{-2}$.
[b] length of the cylinders (fitted).
[c] radius of the cylinders (fitted).
[d] linear density (fitted according to reference 1).

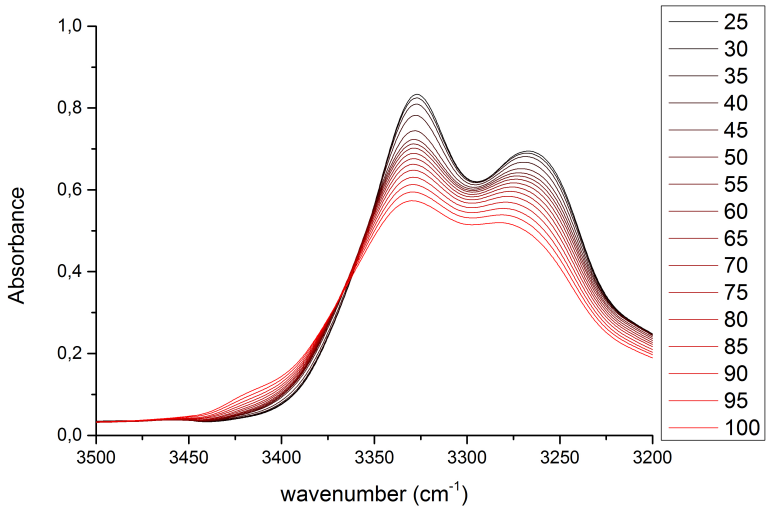

Figure S2. VT-FTIR spectra for solutions of bisurea **B** in toluene (10 mM). The free N-H stretching vibration is visible at high temperatures at ca. 3420 cm^{-1}.[2]

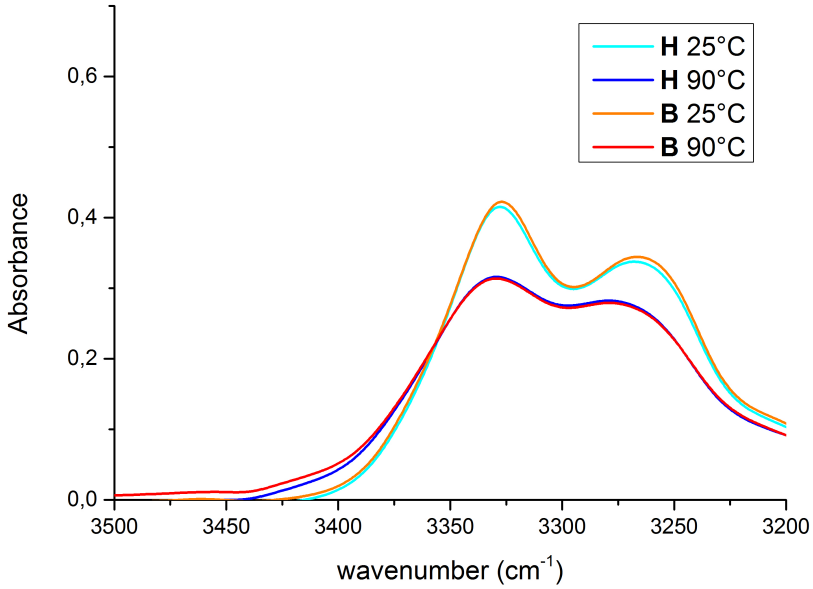

Figure S3. VT-FTIR spectra for solutions of bisurea **B** or **H** in toluene (10 mM).

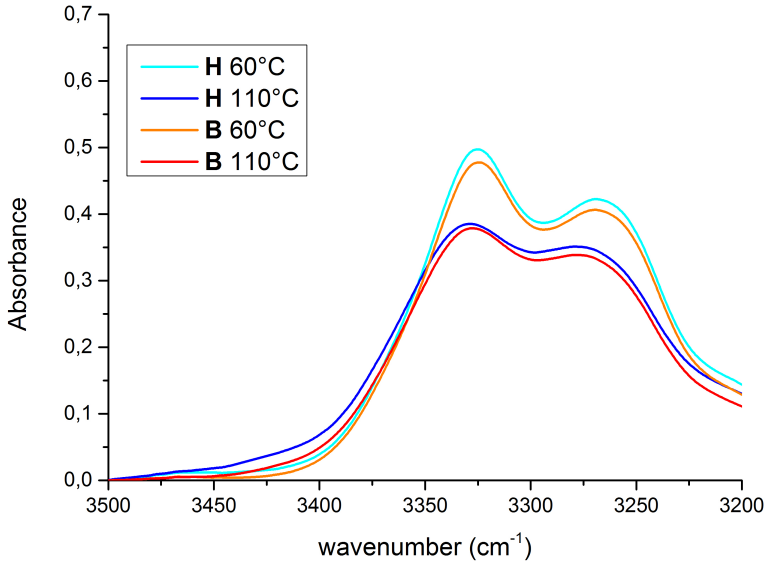

Figure S4. VT-FTIR spectra for solutions of bisurea **B** or **H** in 1-chlorohexane (10 mM).

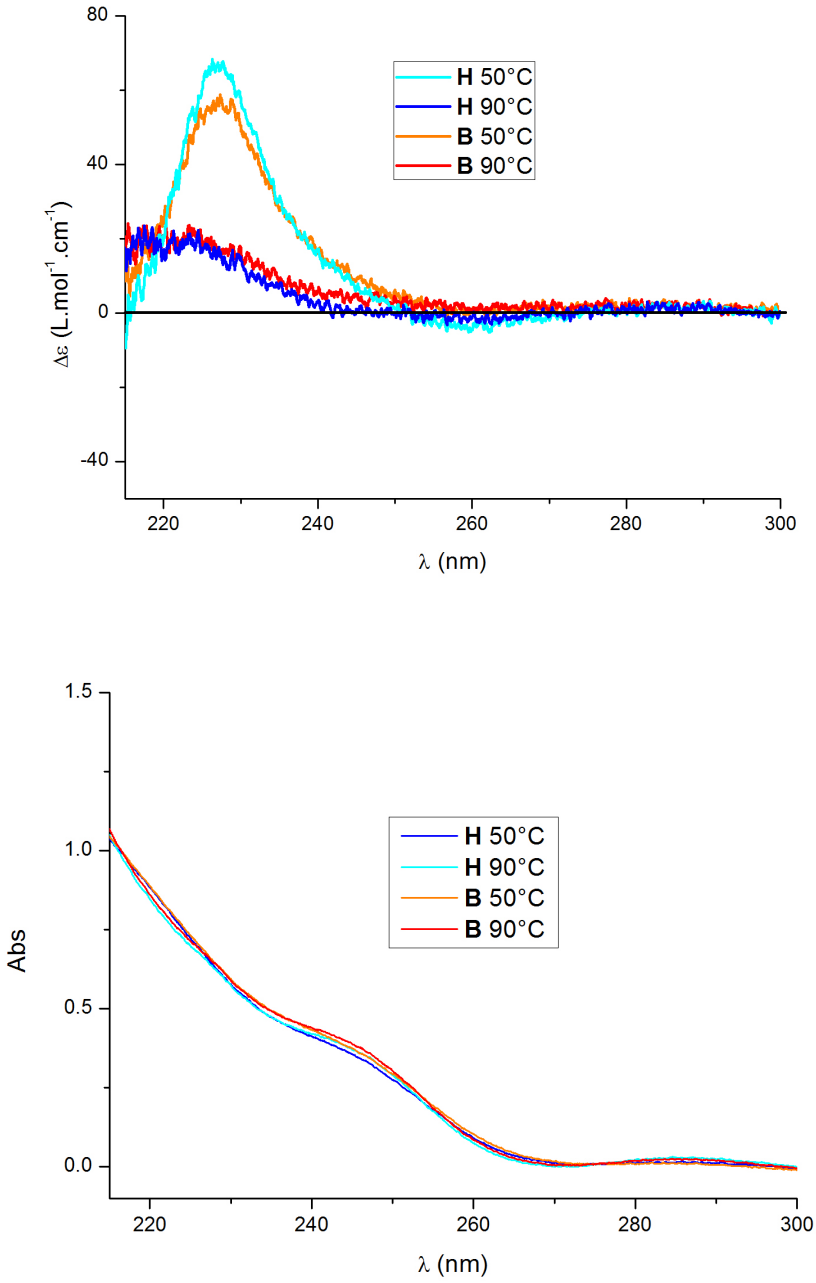

Figure S5. VT-CD (top) and VT-UV (bottom) spectra for solutions of bisurea **B** or **H** in 1-chlorodecane (0.1 mM).

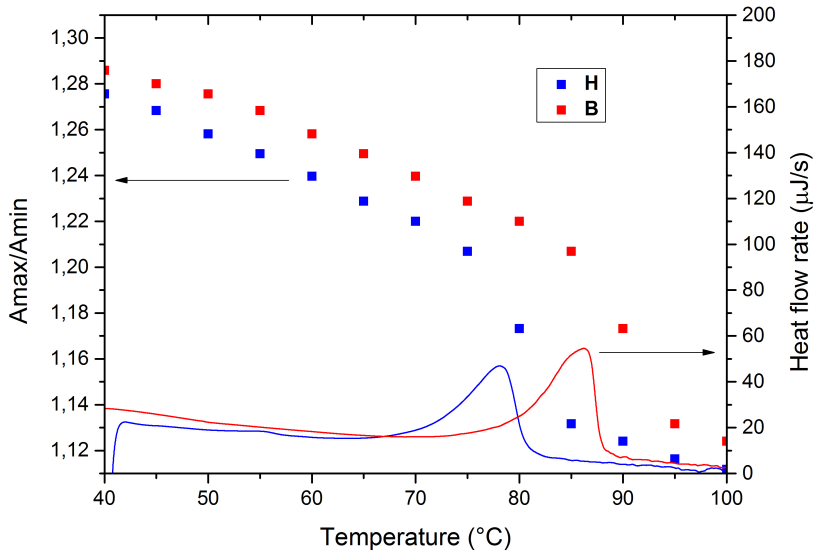

Figure S6. DSC thermogram and IR absorbance ratio (measured at 3325cm^{-1} (max) and 3295cm^{-1} (min)) for solutions of bisurea **B** or **H** in 1-chlorohexane (10 mM, heating run, 1°C/min).

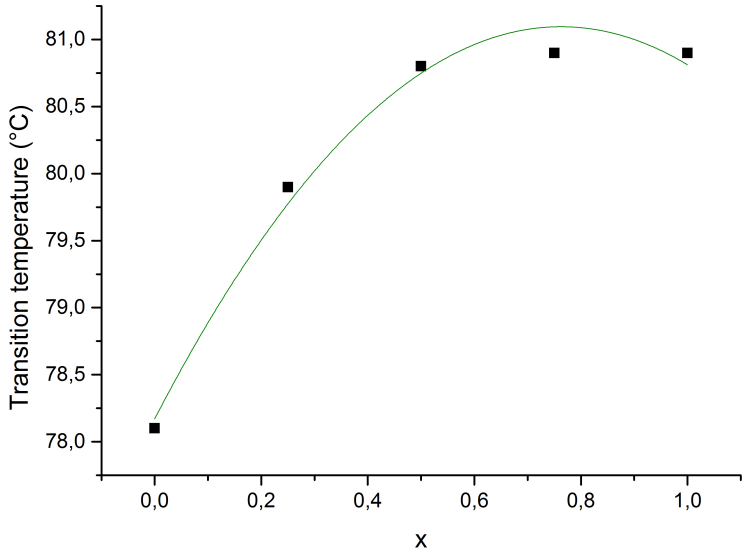

Figure S7. Transition temperature for mixtures of bisureas **C** and **H** in 1-chlorohexane (10 mM measured by nDSC). x=0 is pure **H**; x=1 is pure **C**; the full line represents the best fit with equation (27).

Table S3. Values (J/mol) for the free energies (per CX_3 group) of $CBr_3\cdots CBr_3$ ($\boldsymbol{G_{BB}^{solv}}$), $CBr_3\cdots CH_3$ ($\boldsymbol{G_{BH}^{solv}}$), $CCl_3\cdots CCl_3$ ($\boldsymbol{G_{CC}^{solv}}$) or $CCl_3\cdots CH_3$ ($\boldsymbol{G_{CH}^{solv}}$) interactions in 1-chlorohexane or 1-bromoheptane solvents, deduced from the fits of Figures 7 and S7. The uncertainty of the calorimetric measurement is ±10 J/mol. *The free energies are normalized by the number of CX_3 groups, so that they actually correspond to half of a $CX_3\cdots CX_3$ interaction.*

$G_{BB}^{Clhexane}$	$G_{BH}^{Clhexane}$	$G_{CC}^{Clhexane}$	$G_{CH}^{Clhexane}$
-120	-140	-30	-50
$G_{BB}^{Brheptane}$	$G_{BH}^{Brheptane}$		
-60	-30		

Table S4. Average values (J/mol) for the free energies (per CX_3 group) of $CBr_3\cdots CBr_3$ ($\boldsymbol{G_{BB}^{solv}}$) or $CCl_3\cdots CCl_3$ ($\boldsymbol{G_{CC}^{solv}}$) interactions in 1-chloroalkane solvents, deduced from Figure 8. The uncertainty of the calorimetric measurement is ±10 J/mol. *The free energies are normalized by the number of CX_3 groups, so that they actually correspond to half of a $CX_3\cdots CX_3$ interaction.*

$G_{BB}^{Clalkane}$	$G_{CC}^{Clalkane}$
-125	-50

Molecular simulations.

Methodology

In order to correctly sample and assess the intermolecular interactions taking place in the supramolecular aggregates, a proper description of the interaction potential via tailored force fields is necessary. The bisurea core aggregation was already successfully modeled and characterized recently,[3] but the XB itself, i.e., the main objective of the present study, is not included in the commonly available force fields.

For that reason, we first performed a tailored parameterization to include XB interactions in the Dreiding force field.[4] Halogen bonding is due to the interaction between an electron-poor area, opposite to the halogen σ-bond, and an electron donor (for instance another halogen atom), as represented in Figure S8. The way to model that interaction, as suggested by the Hozba group, is to include a dummy positive point charge beyond the nucleus of the halogen atom and opposite to the σ-bond.[5] However such a strategy leaves two parameters to tailor, namely the value of the point charge and its distance from the halogen nucleus.

Figure S8. Electrostatic potential mapped onto the iso-electronic-density (value = 0.0004 u.a.) surface of the model molecule CH_3-CBr_3 computed at the B3LYP/6-31+G** level of theory. The electrostatic potential ranges from -1.805×10^{-2} u.a. (red) to $+2.805 \times 10^{-2}$ u.a. (blue). Carbon atoms are depicted in grey, hydrogen atoms in white and bromine atoms in red. Left: transparent surface showing the geometry. Right: Solid surface showing the electrostatic potential. The σ-hole is represented by the light blue disk surrounded by the green circle in the extension of each C-Br bond.

In order to define a good parameterization, the interactions with dimers of CH_3X have been calculated by quantum chemical methods (DFT and MP2). These calculations were performed using Second-Order Møller-Plesset (MP2) and Density Functional Theory (DFT) methods with the triple-zeta 6-311G(d,p) basis set including polarization functions on all the atoms. The range-separated, dispersion-corrected wB97X-D exchange-correlation functional was used for the DFT calculations. The obtained potential energy was fitted with a Dreiding potential that uses PCFF[6,7] charges, by adjusting the two parameters. The best fit was obtained for a point charge of +0.2, and an equilibrium distance of 1.2 Å. To maintain the electroneutrality of the molecule, the PCFF charge located on the bromine atomic centers was decreased by 0.2.

To investigate the structure of the single and double filaments of the bisurea systems, the Materials Studio modeling package (from Biovia, formerly Accelrys) was used. We built assemblies of 32 molecules and performed a conformational search varying the periodical motif along the assembly direction. The long-range interaction cutoff distance was set to 14 Å with a spline width of 3 Å. The assemblies were first optimized by molecular mechanics,

using a conjugate gradient algorithm with a convergence criterion of 0.001 kcal/mol.Å. Then, MD simulations of 1500 ps were performed in the NVT ensemble, using a Nosé[8] thermal bath with a coupling constant of 0.1 to maintain the temperature at 300 K. A Verlet velocity algorithm[9] was used to integrate the equations of motion with a 1 fs time step.

These studies were performed without an explicit solvent, and on assemblies where the long side chains were replaced by methyl groups (Chart S1). These approximations, made to alleviate the computational cost, are based on the reasonable assumption that the structure of the filaments is mainly derived from intermolecular interactions taking place at the level of the bisurea cores (notably via hydrogen bonds and steric hindrance). However, to study the weak XB interactions between the brominated extremities of long alkyl side-chains, as found in bisurea **B**, the side chains and explicit solvent molecules have to be included in the model. This has been made for the most stable assembly of the single filament, and that of the double filament. A periodic motif of the filament was oriented along the *a* dimension of an orthorhombic box filled with 1-chlorohexane as a solvent. *a* was set to the length of the periodic motif, and *b* and *c* were set to avoid close interactions with filament images. The box was relaxed by MM, then submitted to a NPT dynamics for 300 ps with a Parrinello barostat, which allows all the cell parameters to vary, to obtain a guess density. Then, the cell parameters of the initial orthorhombic box were adapted to reach the guess density (see Table S5), the box was relaxed with the cell angles maintained fixed, and a NPT dynamics of 20 ns at 300 K was performed, this time with a Berendsen barostat to maintain the orthorhombicity of the cell. The Nosé[8] thermal bath was used with a coupling constant of 0.1 and the equations of motion were integrated by a Verlet velocity algorithm[9] with a 1 fs time step.

Table S5. Initial parameters of the simulation box for the single and double filaments in explicit solvent.

	a	*b*	*c*	Number of bisurea	Number of 1-chlorohexane
Single filament	38.8	79.8	79.8	10	852
Double filament	62.1	87.0	87.0	32	1546

CD spectra were calculated for the different assemblies, using an excitonic model. In short, a supramolecular Hamiltonian was built on the basis of localized excited states. Those states were obtained from CIS calculations performed on isolated molecules using the ZINDO parameterization implemented in the Gaussian package.[10] To ensure the convergence of the spectra up to 180 nm, 60 excited states have been considered. After diagonalization of this Hamiltonian, supramolecular transition dipole and magnetic moments were calculated and used to compute the oscillator and rotatory strengths.

Results

For single filaments, each monomer interacts by H-bonding with its two neighbors in the stack. A previous study[3] showed that the urea groups are tilted with respect to the aromatic core by ca. |140|°, and that the sign of the torsion can flip from one monomer to the next along the assembly axis, thus giving rise to *n*x*m* periodical motifs (*n* is the number of successive monomers with torsions of one sign, followed by *m* successive monomers with torsions of the opposite sign). When *n* is infinite and *m* is 0 (or the opposite), a helix is obtained. See Figure S9, top-left panel, rightmost structure. Here, we compared the stability of the single helix

structure (M-helix), and of the 1x1, 2x2 and 3x3 structures, (some of them were discussed in a previous publication for other bisurea molecules[3]).

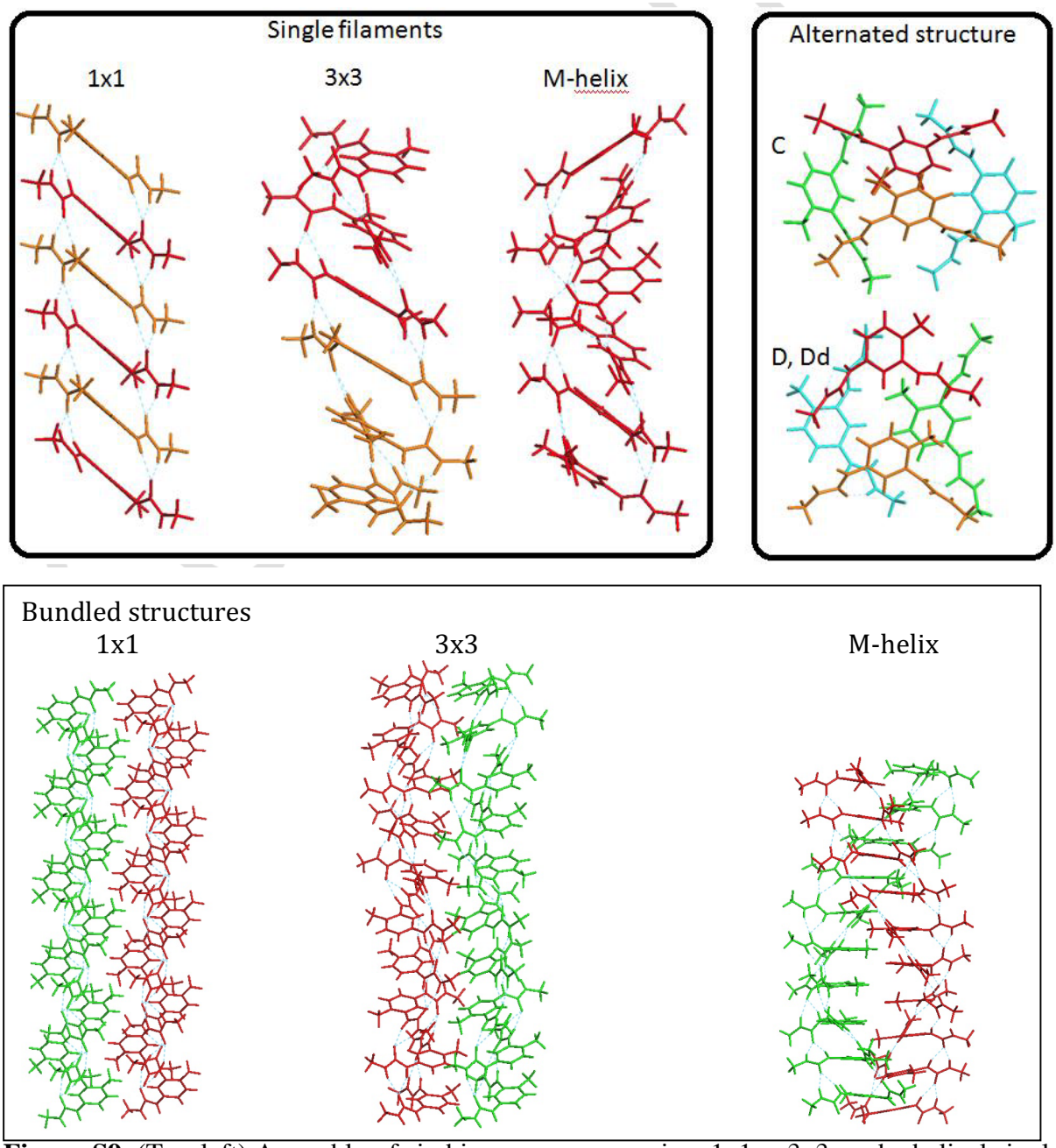

Figure S9. (Top-left) Assembly of six bisurea monomers in a 1x1, a 3x3, and a helical single filament; the monomers in red (orange) have a positive (negative) sign for the dihedral angle responsible of the orientation of the urea with respect to the core. (Top-right) Motifs for double filaments (alternated structures) where each monomer forms hydrogen bonds with four neighboring molecules. In Dd, the motif of four molecules is adjoined by another one on top of it (not represented), and rotated by 180°. (Bottom) Assembly of twenty bisurea monomers in double filaments (bundled structures), based on two interacting 1x1, 3x3 or helical single filaments (one in red, the other one in green).

For double filaments, we evaluated two categories of assemblies. The first category (named alternated structures) is composed of structures where each monomer interacts by hydrogen bonds with four neighboring molecules, instead of two in a single filament. Three such assemblies, called C, D and Dd, were investigated, see Figure S9, top-right. The second

category (named bundled filament structures) is based on two single filaments maintained together by their long-range interactions. Bundled filament structures based on the M-helix (composed of two intertwined single filaments), and on the 1x1, 2x2, and 3x3 structures (composed of two single filaments located next to each other) were investigated.

Following the methodology described above to generate the conformations, we then performed 1500 ps MD, and compared the various filaments for **h** (Chart S1), which is a good approximation of the **H** molecule (the C11 alkyl chain was replaced by a methyl group for alleviating the computational cost).

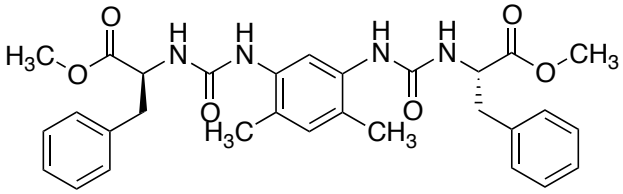

Chart S1. Structure of model bisurea **h**.

The energy analyses (Figure S10) show that the helical arrangement of the bisurea monomers led to the most stable structures in both the single and double filament assemblies. In addition, the simulated CD spectra (Figure S11) show that the helical structures have intense bisignated signals with a positive band at ca. 210 nm followed by a negative one at ca. 205 nm. Such a pattern is closest to the experimental CD spectrum for the related molecule **H** (Figure S5), although with different relative intensities, which could result from the high temperature at which the experiment was performed (50-90°C) when compared to the simulation temperature (27°C). The other simulated structures have either a signal that has no resemblance to the experimental results or a featureless CD signal, especially the other double filament structures proposed, and the filaments with *mxm* motifs, as the helicity is reversed every *m* molecules along the filament. The helical filaments, both single and double, thus appear as good candidates to explain the experimental results.

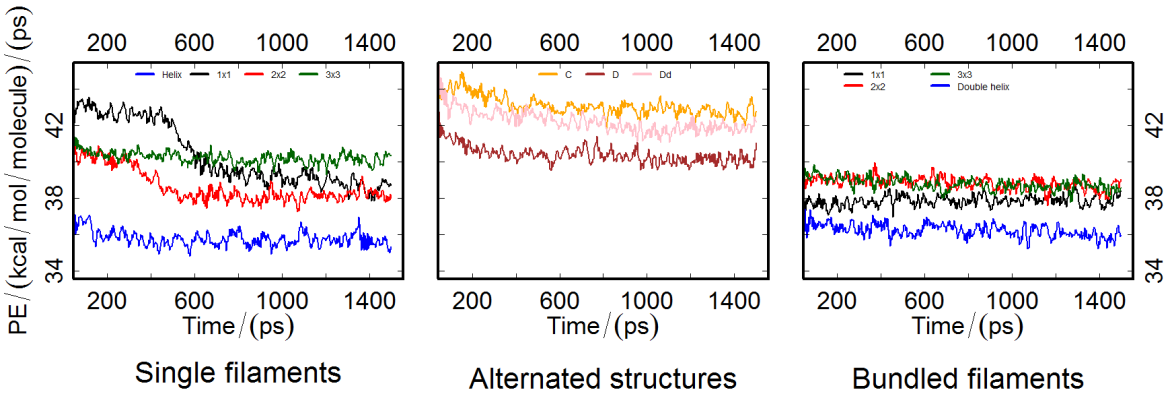

Figure S10. Evolution of the potential energy of the different structures of single and double filaments during 1500 ps MD. The reference energy level is arbitrary.

We thus focused on the single and double helix structures, which are displayed in Figure S12. They have a linear density of ca. 0.25 $Å^{-1}$ and 0.54 $Å^{-1}$, respectively. These values can be compared to the experimental assemblies for the related molecule **H** and **B**, which, according to SANS data (Table S2) have both a linear density of ca. 0.18 $Å^{-1}$ at 65°C (single filament) and 0.48 $Å^{-1}$ at 20°C (double filament).

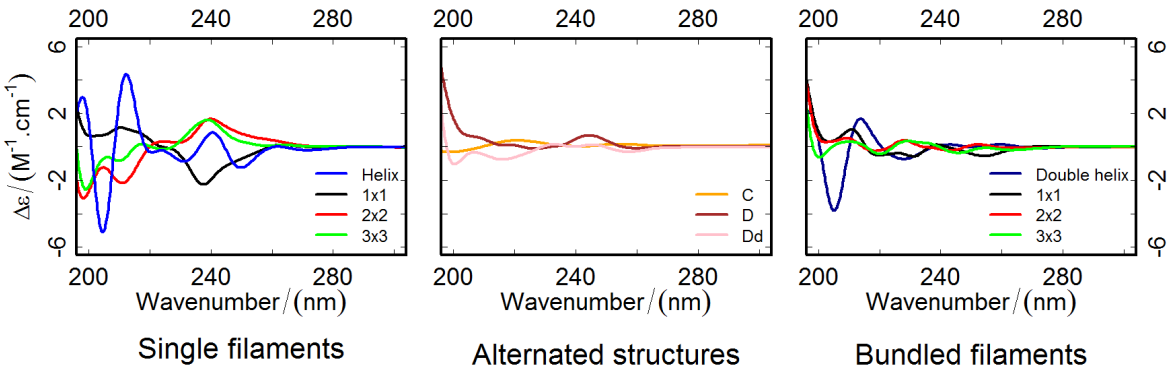

Figure S11. Simulated CD spectra of the single and double filaments for bisurea **h**.

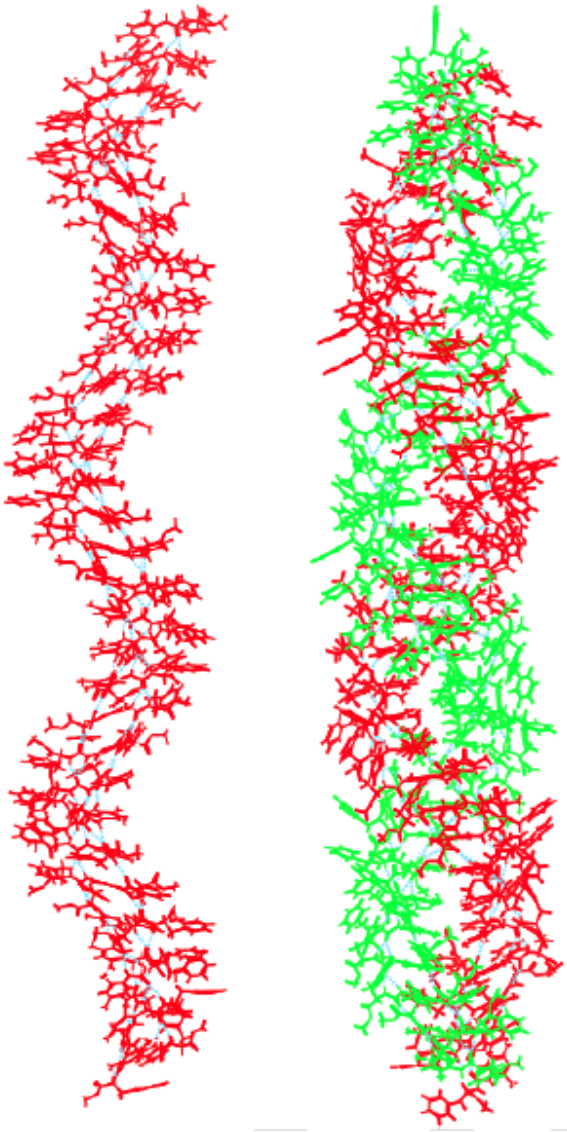

Figure S12. Representative structure of the helical single (left) and double (right) filaments for bisurea **h** generated during MD. The H-bonds are represented in pale blue.

To characterize their hydrogen bond network, we calculated the radial distribution function between the hydrogen atoms of the urea moieties and the oxygen atoms of either the urea, or the ester moieties (to assess whether they participate to the H-bond pattern). The peak at 3Å corresponds to intramolecular distances, and the one at 2 Å corresponds to the hydrogen bonds. The peak at 2 Å is very intense for urea, and almost absent for ester in the single filament and in the double filament (Figure S13). To quantify the proportion of hydrogen bonds with both acceptors, we calculated the cumulative number of oxygen atoms, n_O, found as a function of the distance from the hydrogen atoms of the urea moieties. At 2.5 Å, a threshold below which most hydrogen bonds take place, the proportion of hydrogen involved in bonds with ester groups is found to be very small: 0.6% and 3.1% for the single and double filaments, respectively. Most hydrogen bonds thus occur with the urea moieties, shown by $n_{O\ urea}$ (full red lines) jumping from 0 to 1 at 2 Å. In agreement with the experimental FTIR results on **H** (Figure S3), these results show that all urea hydrogen atoms are involved in hydrogen bonds (except the hydrogen atoms belonging to the monomer(s) located at one end of the helix).

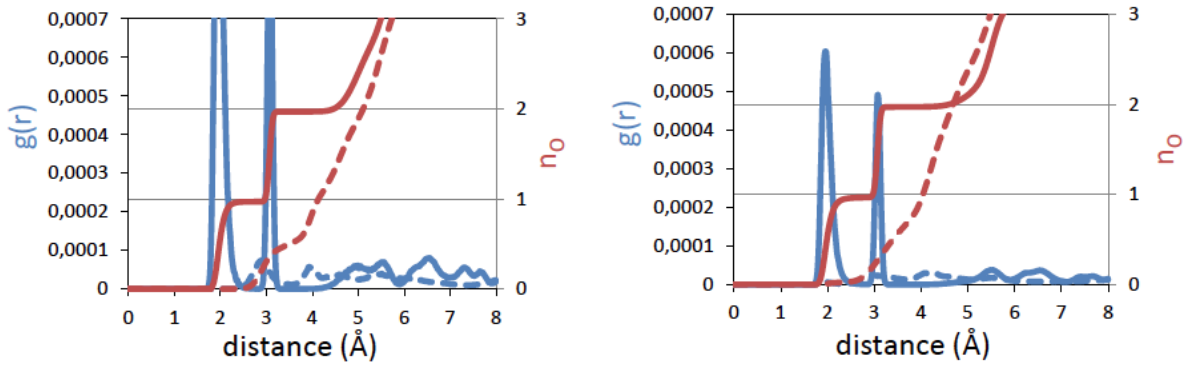

Figure S13. Radial distribution function, g(r), between H_{urea} and O, and cumulative number of O, n_O, around H_{urea} as a function of the H_{urea}-O distance, for the single (left) and double (right) filaments of bisurea **h**. The oxygen atoms are either O_{urea} (full lines) or O_{ester} (dashed lines).

The study of bisurea **B** in 1-chlorohexane shows that neither the introduction of long brominated alkyl chains nor the solvent change significantly the parameters of the core of the filaments: the helical single and double filaments have a linear density of ca. 0.26 $Å^{-1}$ and 0.52 $Å^{-1}$, respectively; the proportion of urea hydrogens involved in hydrogen bonds with urea is 99.7 and 99.1%, respectively, and with ester is 1.4% and 1.5%, respectively; simulated CD spectra (Figure S14) show that the helical structures have intense bisignated signals with a positive band at ca. 210 nm followed by a negative one at ca. 205 nm.

Hence, both experimental data (SANS, CD, IR) and theoretical data indicate that bisurea **B** and **H** have similar structures for the core of the filaments, which are thus not influenced by the nature of the end-groups. This result is not surprising, as the chemical modifications are made at the extremities of the molecules, far from the core of the molecules where the interactions driving the assembly take place.

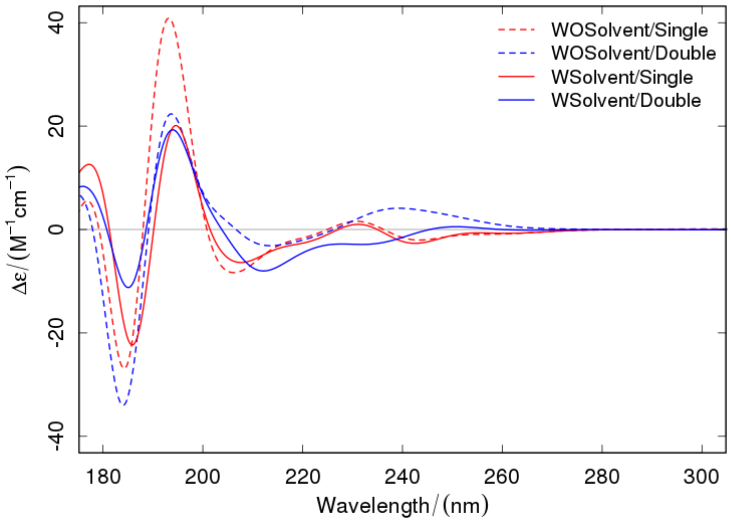

Figure S14. Simulated CD spectra of the single and double filaments for bisurea **B** without or with solvent.

Figure S15 (top) shows the radial distribution functions calculated between Br atoms (from which the vicinal Br atoms have been excluded). The first peak at 3.8Å corresponds to direct contacts between Br atoms belonging to different molecules. The cumulative number of Br atoms located at a given distance from a given Br atom have been extracted from these distributions, and Figure S15 (bottom) shows the ratio of this cumulative number in the double filament, normalized by the corresponding value in the single filament. The data show that there are about 3 times more Br···Br contacts in the double filament than in the single filament (about 0.74 and 0.25 contacts per Br, respectively, when integrating the first peak up to the minimum at 5.2Å). This result is consistent with the denser packing in the double filament structure and is in agreement with the monitoring of the distance between CBr_3 groups (Figure 4). The quantitative difference between the absolute numbers of CBr_3 contacts (Figure 4) and Br···Br (Figure S15) contacts is due to the fact that one CBr_3 group can be involved in several Br···Br contacts.

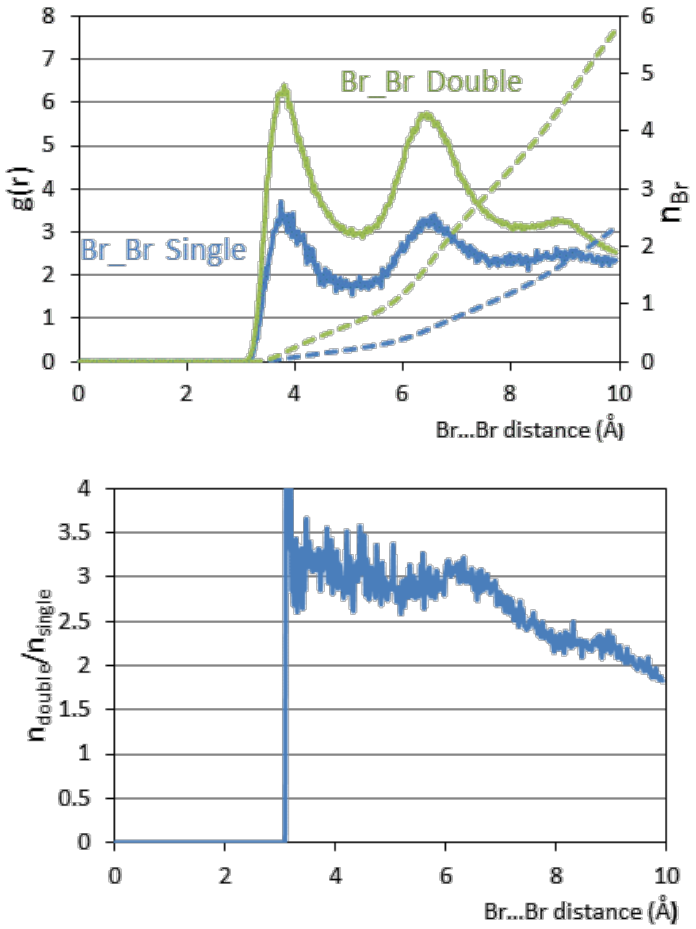

Figure S15. Top: Intermolecular radial distribution function, g(r), between Br atoms (continuous line), and cumulative number of neighboring Br (dotted line) as a function of the Br···Br distance, for the single (blue lines) or double (green lines) filaments. Bottom: Ratio of the cumulative numbers of neighboring Br for the single and double filaments as a function of the Br···Br distance.

Synthesis.

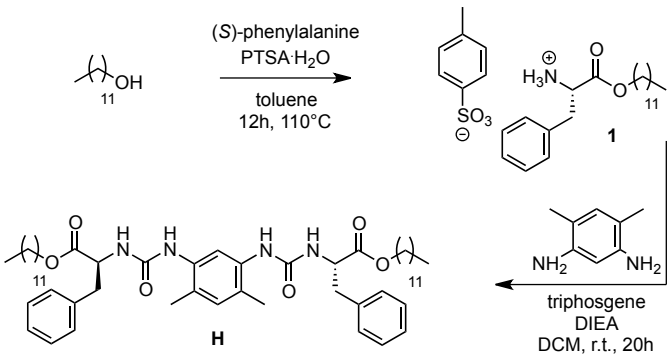

Scheme S1. Synthesis of reference bisurea **H**.

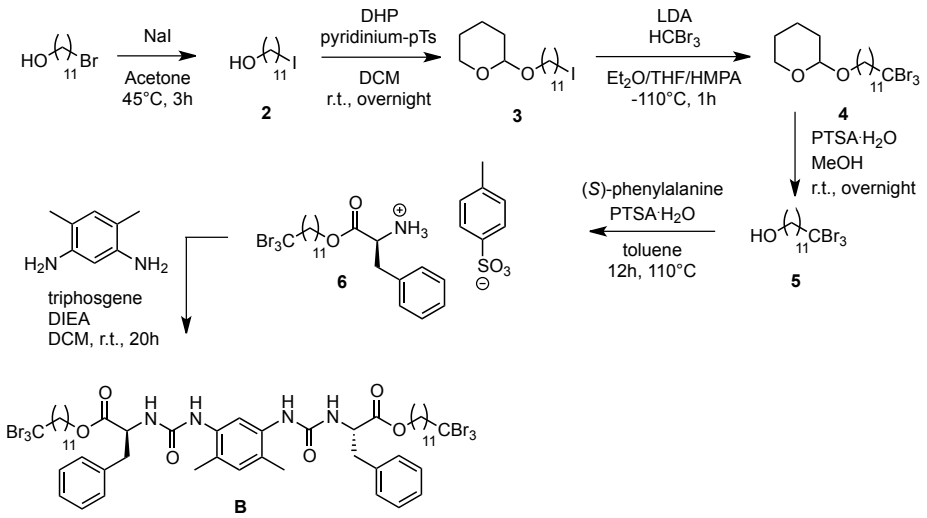

Scheme S2. Synthesis of brominated bisurea **B**.

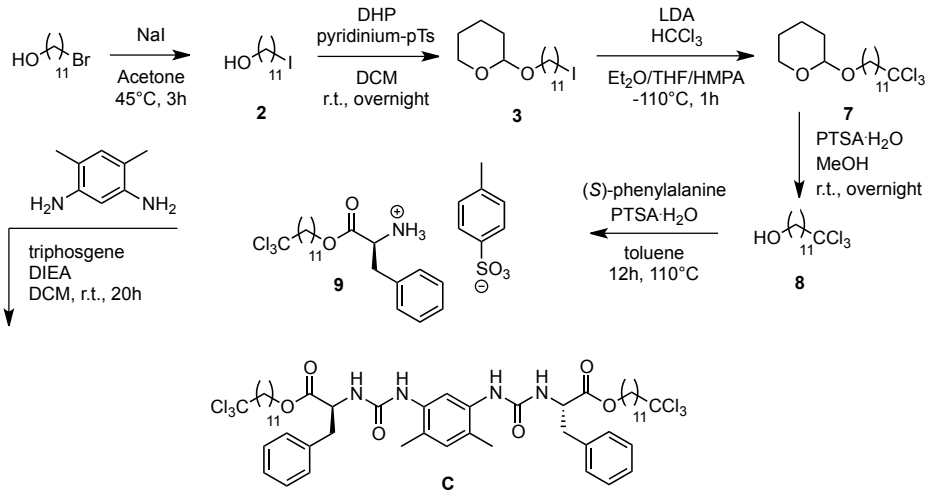

Scheme S3. Synthesis of chlorinated bisurea **C**.

General synthetic methods

All amino acids were purchased from Sigma-Aldrich or Alfa Aesar (99% purity) and used as received. 2,4-Toluenediisocyanate (TDI) was purchased from Sigma Aldrich (purity ≥ 98%) and was used directly.

Chromatography-grade solvents were used as received. Dried CH_2Cl_2 and THF were obtained from an SPS solvent purification system (IT-Inc) and stored on 4Å molecular sieves. NEt_3 and diisopropylethylamine (DIEA) were dried by distillation over CaH_2 and stored over 4Å molecular sieves.

Flash chromatography purification was made with a Grace Reveleris set-up and columns of the same brand. The water was purified using a milli-Q system.

NMR spectra were recorded on a Bruker Avance 400 or 300 spectrometers and calibrated to the residual solvent peak. Peaks are reported in ppm with their corresponding multiplicity (s: singlet; d: doublet, t: triplet; q: quartet; quint: quintet; hept: heptuplet; dd: doublet of doublets; dt: doublet of triplets; td: triplet of doublets), integration, and respective *J* coupling constants are given in hertz. Exact mass measurements (HRMS) were obtained on TQ R30-10 HRMS spectrometer by ESI+ ionization and are reported in m/z for the major signal.

2 (11-iodoundecanol). Adapted from the literature.[11]

11-bromoundecanol (7.4 g, 29.4 mmol, 1.0 eq.) was added to a 0.5 M solution of NaI in acetone (65 mL). The mixture was stirred at room temperature for 3h. A NaBr precipitate was observed. The mixture was extracted with CH_2Cl_2 and washed with water. The organic phase was dried with $MgSO_4$ and concentrated under reduced pressure. Purification by flash chromatography (10% ethylacetate/petroleum ether (PE)) provided the pure product (8.3 g, 95%) as a slightly yellow crystalline powder.

^{1}H NMR (300 MHz, $CDCl_3$) δ 3.63 (t, 2H, HO-CH_2, J = 6.5 Hz), 3.19 (t, 2H, I-CH_2, J = 6.8 Hz), 1.83 (p, 2H, HO-CH_2-CH_2, J = 7.1 Hz), 1.57 (p, 2H, I-CH_2-CH_2, J = 6.7 Hz), 1.45-1.25 (m, 14H, CH_2)

^{13}C{^{1}H} NMR (101 MHz, $CDCl_3$) δ 63.2, 33.7, 32.9, 30.6, 29.7, 29.6, 29.5, 29.5, 28.7, 25.9, 7.4.

3 (2-(11-iodoundecyloxy)tetrahydropyran). Adapted from the literature.[12]

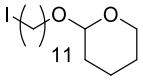

11-iodoundecanol (**2**, 8.3 g, 28.0 mmol, 1.0 eq.) and pyridinium *p*-toluene sulfonate (1.06 g, 4.2 mmol, 0.15 eq.) were dissolved in CH_2Cl_2 (0.5 M) and dihydropyran (3.6 mL, 42 mmol, 1.5 eq.) was added to the mixture. The mixture was stirred at room temperature overnight in the dark. The mixture was then concentrated under reduced pressure. Purification by flash chromatography (50% CH_2Cl_2/PE) provided the pure product (9.7 g, 91%) as a colorless oil.

^{1}H NMR (300 MHz, $CDCl_3$) δ 4.58 (t, 1H, O-CH-O, J = 3.0 Hz), 3.70 (AB spin system, 2H, O-CH_2, J = 70.3 Hz), 3.56 (AB spin system, 2H, O-CH_2, J = 59.8 Hz), 3.19 (t, 2H, I-CH_2, J = 7.1 Hz), 1.90-1.68 (m, 2H, CH_2), 1.68-1.48 (m, 2H, CH_2), 1.48-1.25 (m, 20H, CH_2).

^{13}C{^{1}H} NMR (75 MHz, $CDCl_3$) δ 98.8, 67.6, 62.3, 33.6, 30.8, 30.5, 29.7, 29.5, 29.4, 29.4, 28.5, 26.2, 25.5, 19.7, 7.2.

HRMS (ESI, m/z) 405.1264 $[M + Na]^+$, 405.1261 calculated for $C_{16}H_{31}IO_2Na$.

4 (2-(12-tribromododecyloxy)tetrahydropyran). Adapted from the literature.[13]

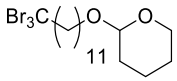

Under Ar atmosphere, a 0.33 M solution of diisopropylamine (7.5 mL, 52.5 mmol, 3.3 eq.) in a 50/50 mixture of THF and Et_2O was cooled to -110°C (ethanol bath) and 29.8 mL of *n*-BuLi (1.6 M in hexane, 47.7 mmol, 3.0 eq.) was added dropwise. $HCBr_3$ (4.2 mL, 47.7 mmol, 3.0 eq.) in a 2/1/1 mixture of THF, Et_2O and HMPA (31 mL in total) was added to the solution. The reaction mixture was then warmed to -80°C by adding acetone to the bath and 2-(11-iodoundecyloxy)tetrahydropyran (**3**, 6.07 g, 15.9 mmol, 1.0 eq.) in THF (20 mL) was added to the mixture. After 30 min the mixture was warmed to room temperature. The mixture was then quenched with a saturated NH_4Cl aqueous solution and extracted with Et_2O. The organic phase was dried with $MgSO_4$ and concentrated under reduced pressure. Purification by flash chromatography (40% CH_2Cl_2/PE) provided the pure product (7.4 g, 92%) as a brown oil.

^{1}H NMR (300 MHz, $CDCl_3$) δ 4.58 (t, 1H, O-C*H*-O, *J* = 3.0 Hz), 3.70 (AB spin system, 2H, O-CH_2, *J* = 70.3Hz), 3.56 (AB spin system, 2H, O-CH_2, *J* = 59.8Hz), 2.98 (t, 2H, CBr_3-CH_2, *J* = 7.8 Hz), 1.90-1.68 (m, 2H, CH_2), 1.68-1.48 (m, 2H, CH_2), 1.48-1.25 (m, 20H, CH_2).

^{13}C{^{1}H} NMR (101 MHz, $CDCl_3$) δ 99.0, 67.8, 62. 5, 60.1, 42.8, 30.9, 29.9, 29.7, 29.7, 29.6, 29.6, 29.6, 29.4, 28.0, 26.4, 25.7, 19.8.

HRMS (ESI, m/z) 528.9750 $[M + Na]^+$, 528.9746 calculated for $C_{17}H_{31}Br_3O_2Na$.

7 (2-(12-trichlorododecyloxy)tetrahydropyran). Adapted from the literature.[13]

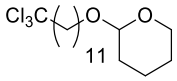

Under Ar atmosphere, a 0.33 M solution of diisopropylamine (2.5 mL, 17.3 mmol, 3.3 eq.) in a 50/50 mixture of THF and Et_2O was cooled to -110°C (ethanol bath) and 9.8 mL of *n*-BuLi (1.6 M in hexane, 15.7 mmol, 3.0 eq.) was added dropwise. $HCCl_3$ (1.3 mL, 15.7 mmol, 3.0 eq.) in a 2/1/1 mixture of THF, Et_2O and HMPA (10 mL in total) was added to the solution. The reaction mixture was then warmed to -80°C by adding acetone to the bath and 2-(11-iodoundecyloxy)tetrahydropyran (**3**, 2.0 g, 5.2 mmol, 1.0 eq.) in THF (6.6 mL) was added to the mixture. After 30 min the mixture was warmed to room temperature. The mixture was then quenched with a saturated NH_4Cl aqueous solution and extracted with Et_2O. The organic phase was dried with $MgSO_4$ and concentrated under reduced pressure. Purification by flash chromatography (40% CH_2Cl_2/PE) provided the pure product (1.5 g, 78%) as a colorless oil.

^{1}H NMR (300 MHz, $CDCl_3$) δ 4.58 (t, 1H, O-C*H*-O, *J* = 3.0 Hz), 3.70 (AB spin system, 2H, O-CH_2, *J* = 70.3 Hz), 3.56 (AB spin system, 2H, O-CH_2, *J* = 59.8 Hz), 2.67 (t, 2H, CCl_3-CH_2, *J* = 8.0 Hz), 1.90-1.68 (m, 2H, CH_2), 1.68-1.48 (m, 2H, CH_2), 1.48-1.25 (m, 20H, CH_2).

^{13}C{^{1}H} NMR (75 MHz, $CDCl_3$) δ 100.2, 98.8, 67.7, 62.3, 55.2, 30.8, 29.8, 29.5, 29.5, 29.5, 29.4, 29.3, 28.3, 26.4, 26.2, 25.5, 19.7.

5 (12-tribromododecanol). Adapted from the literature.[13]

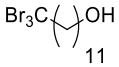

2-(12-tribromododecyloxy) tetrahydropyran (**4**, 1.0 g, 2.0 mmol, 1.0 eq.) and PTSA·H_2O (0.04 g, 0.2 mmol, 0.1 eq.) were mixed in methanol (75 mL) overnight. The mixture was diluted in CH_2Cl_2 and washed with brine. The organic phase was dried with $MgSO_4$ and concentrated under reduced pressure. Purification by flash chromatography (40% CH_2Cl_2/PE) provided the pure product (0.8 g, 98%) as a colorless oil.

^{1}H NMR (300 MHz, $CDCl_3$) δ 3.64 (t, 2H, HO-CH_2, *J* = 6.5 Hz), 2.98-2.94 (m, 2H, CBr_3-CH_2), 1.90-1.68 (m, 2H, HO-CH_2-CH_2), 1.68-1.48 (m, 2H, CH_2), 1.48-1.25 (m, 14H, CH_2).

^{13}C{^{1}H} NMR (101 MHz, $CDCl_3$) δ 63.2, 60.1, 42.8, 32.9, 29.7, 29.6, 29.6, 29.5, 29.5, 29.4, 28.0, 25.9.

8 (12-trichlorododecanol). Adapted from the literature.[13]

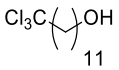

2-(12-trichlorododecyloxy)tetrahydropyran (**7**, 1.5 g, 3.9 mmol, 1.0 eq.) and PTSA·H_2O (0.08 g, 0.4 mmol, 0.1 eq.) were mixed in methanol (150 mL) overnight. The mixture was diluted in CH_2Cl_2 and washed with brine. The organic phase was dried with $MgSO_4$ and concentrated under reduced pressure. Purification by flash chromatography (40% CH_2Cl_2/PE) provided the pure product (0.4 g, 37%) as a colorless oil.

^{1}H NMR (400 MHz, $CDCl_3$) δ 3.63 (t, 2H, HO-CH_2, *J* = 6.6 Hz), 2.69 – 2.62 (m, 2H, CCl_3-CH_2), 1.76 (ddd, 2H, HO-CH_2-CH_2, *J* = 11.6, 9.4, 6.1 Hz), 1.62 – 1.51 (m, 2H, CH_2), 1.47 – 1.23 (m, 14H, CH_2).

^{13}C{^{1}H} NMR (101 MHz, $CDCl_3$) δ 63.0, 55.2, 32.8, 29.5, 29.5, 29.4, 29.4, 29.3, 28.3, 26.4, 25.7.

Synthesis of ester ammonium tosylate salts (Method A)

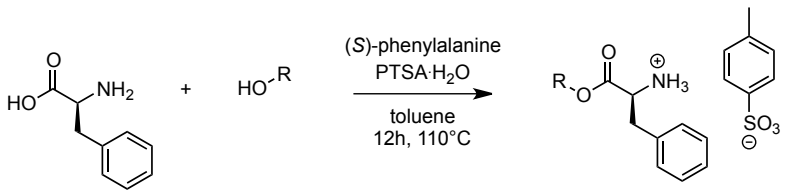

The synthesis was adapted from the literature:[14] (*S*)-Phenylalanine (1.0 eq.), the alcohol (1.1 eq.) and PTSA·H_2O (1.1 eq.) were mixed in toluene (0.15 M) and then stirred under reflux equipped with a Dean-Stark apparatus for 12h. The mixture was then concentrated under reduced pressure and diluted in Et_2O. The solution was cooled with ice to precipitate for a couple of hours. The precipitate was then filtered, washed with cold Et_2O and dried under vacuum.

1 (dodecyl (*S*)-phenylalaninate ammonium tosylate salt)

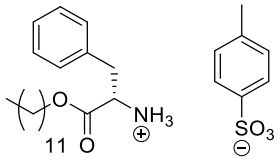

Preparation was achieved following method A using commercially available dodecanol and (*S*)-phenylalanine. **1** (10.6 g, 86%) was obtained pure as a white powder.

^{1}H NMR (400 MHz, $CDCl_3$) δ 8.24 (s, 3H, NH_3), 7.74 (d, 2H, Ar-*H*, *J* = 8.2 Hz), 7.20 – 7.04 (m, 7H, Ar-*H*), 4.29 – 4.19 (m, 1H, NH_3-C*H*), 3.93 – 3.77 (m, 2H, COO-CH_2), 3.24 (dd, 1H, NH_3-CH-CH_2, *J* = 14.0, 5.3 Hz), 3.04 (dd, 1H, NH_3-CH-CH_2, *J* = 14.0, 8.4 Hz), 2.32 (s, 3H, Ar-CH_3), 1.38 – 0.96 (m, 20H, CH_2), 0.89 (t, 3H, CH_3, *J* = 6.8 Hz).

^{13}C{^{1}H} NMR (101 MHz, $CDCl_3$) δ 169.0, 141.7, 140.3, 134.5, 129.6, 128.9, 128.7, 127.3, 126.3, 66.4, 54.3, 36.5, 32.1, 29.8, 29.8, 29.7, 29.6, 29.5, 29.4, 28.2, 25.7, 22.8, 21.4, 14.2.

6 (12-tribromododecyl (*S*)-phenylalaninate ammonium tosylate salt)

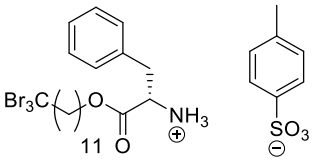

Preparation was achieved following method A using 12-tribromododecanol (**5**) and (*S*)-phenylalanine. **6** (6.6 g, 85%) was obtained pure as a white powder.

^{1}H NMR (300 MHz, $CDCl_3$) δ 8.41 (s, 3H, NH_3), 7.50 (d, 2H, Ar-*H*, *J* = 8.0 Hz), 7.32 (q, 3H, Ar-*H*, *J* = 7.3 Hz), 7.22 (d, 2H, Ar-*H*, *J* = 7.1 Hz), 7.12 (d, 2H, Ar-*H*, *J* = 7.9 Hz), 4.29 (t, 1H, NH_3-C*H*, *J* = 6.9 Hz), 4.02 (t, 2H, COO-CH_2, *J* = 6.4 Hz), 3.09 (d, 2H, NH_3-CH-CH_2, *J* = 21.7 Hz), 2.96 (t, 2H, CBr_3-CH_2, *J* = 7.8 Hz), 2.29 (s, 3H, Ar-CH_3), 1.68 (quint, 2H, COO-CH_2-CH_2, *J* = 7.4 Hz), 1.50-1.08 (m, 16H, CH_2).

^{13}C{^{1}H} NMR (101 MHz, $CDCl_3$) δ 169.0, 141.6, 140.4, 134.4, 129.6, 128.9, 128.7, 127.4, 126.3, 66.4, 60.1, 54.3, 42.8, 36.5, 29.7, 29.6, 29.5, 29.3, 28.2, 28.0, 25.7, 21.5.

HRMS (ESI, m/z) 570.0044 $[M]^+$, 570.0035 calculated for $C_{21}H_{33}Br_3NO_2$.

9 (12-trichlorododecyl (*S*)-phenylalaninate ammonium tosylate salt)

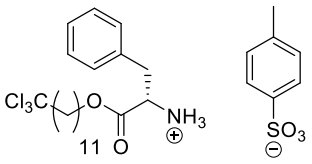

Preparation was achieved following method A using 12-trichlorododecanol (**8**) and (*S*)-phenylalanine. **9** (0.6 g, 76%) was obtained pure as a white powder.

^{1}H NMR (300 MHz, $CDCl_3$) δ 8.22 (s, 3H, N*H*$_3$), 7.74 (d, 2H, Ar-*H*, *J* = 8.2 Hz), 7.21-7.07 (m, 7H, Ar-*H*), 4.35-4.20 (m, 1H, NH_3-C*H*), 3.98-3.82 (m, 2H, COO-C*H*$_2$), 3.17 (d, 2H, NH_3-CH-C*H*$_2$, *J* = 5.9 Hz), 2.67 (t, 2H, CCl_3-C*H*$_2$, *J* = 8.0 Hz), 2.34 (s, 3H, Ar-C*H*$_3$), 1.78 (quint, 2H, COO-CH_2-C*H*$_2$, *J* = 7.4 Hz), 1.48-1.00 (m, 16H, C*H*$_2$).

^{13}C{^{1}H} NMR (101 MHz, $CDCl_3$) δ 169.0, 141.6, 140.4, 134.5, 129.6, 128.9, 128.7, 127.4, 126.3, 66.4, 55.3, 54.4, 36.5, 29.7, 29.6, 29.4, 29.3, 28.5, 28.2, 26.5, 25.7, 21.5.

HRMS (ESI, m/z) 436.1575 $[M]^+$, 436.1571 calculated for $C_{21}H_{33}Cl_3NO_2$.

Synthesis of ester bisureas (Method B)

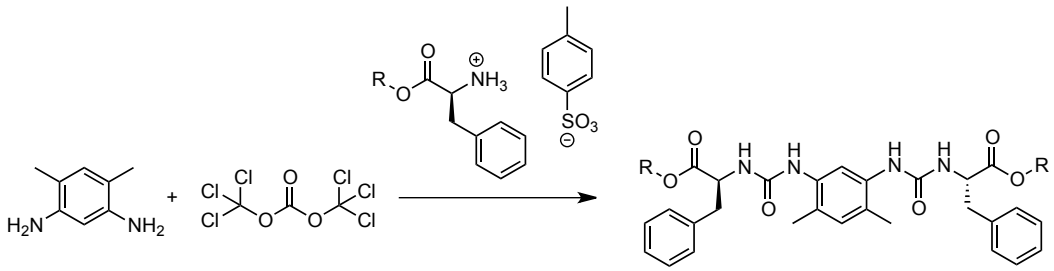

The synthesis was adapted from the literature:[15] Under Ar atmosphere, a 70 mM solution of 4,6-dimethyl-1,3-diaminobenzene (1.0 eq.) and DIEA (2.0 eq.) in CH_2Cl_2 was added at 2.5 mL/h to a 60 mM solution of triphosgene (0.66 eq.) in CH_2Cl_2. The mixture was stirred for 1h after addition and a 0.3 M solution of the ammonium ester (2.1 eq. and of DIEA (6.3 eq.) in CH_2Cl_2 were added to the mixture. After one hour, the solution was concentrated under reduced pressure and purified by recrystallization from acetonitrile.

H

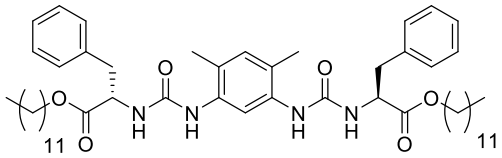

Preparation was achieved following method B using dodecyl (*S*)-phenylalaninate ammonium tosylate salt (**1**). The crude mixture was recrystallized twice from acetonitrile yielding pure **H** (1.49 g, 62%) as a white paste.

^{1}H NMR (300 MHz, DMSO-d_6) δ 7.95 (s, 1H, Ar*H*), 7.75 (s, 2H, N*H*), 7.36-7.15 (m, 10H, Ar*H* and N*H*), 6.85 (s, 1H, Ar*H*), 6.70 (d, 2H, Ar*H*, J = 7.6 Hz), 4.49 (q, 2H, NH-C*H*, J = 6.7 Hz), 4.00 (t, 4H, COO-CH_2, J = 6.2 Hz), 3.08-2.91 (m, 4H, NH-CH-CH_2), 2.05 (s, 6H, Ar-CH_3), 1.50 (q, 4H, COOCH$_2$CH_2, J = 6.0 Hz), 1.30-1.15 (m, 36H, CH_2), 0.85 (t, 6H, CH_3, J = 6.7 Hz).

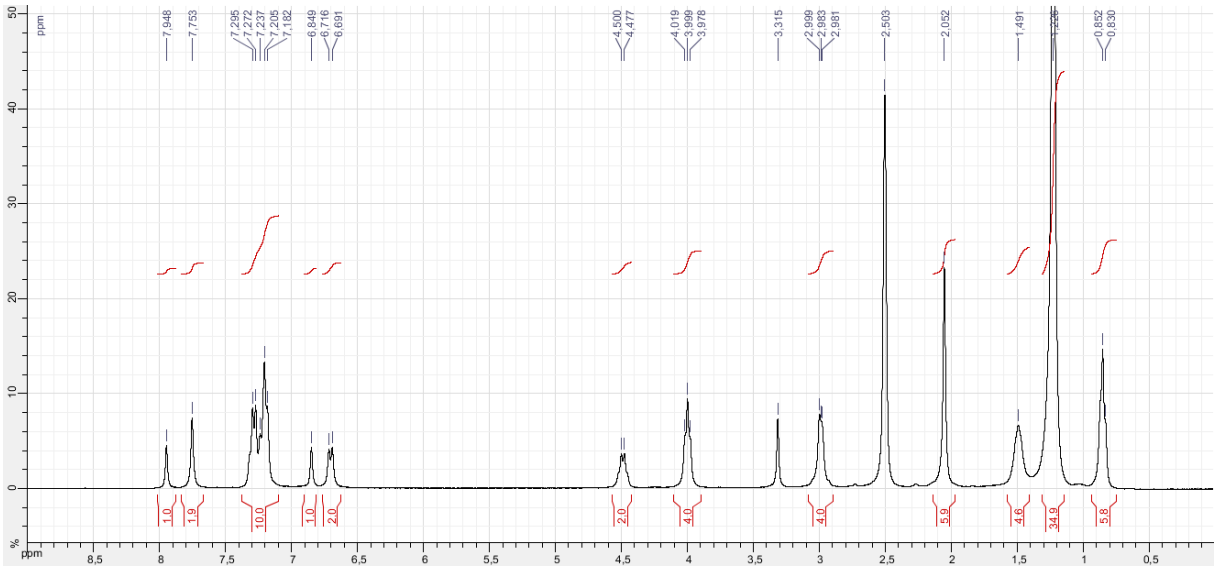

Figure S16. ^{1}H NMR of **H** (300 MHz in DMSO-d_6)

^{13}C{^{1}H} NMR (101 MHz, DMSO-d_6/THF-d_8 2/1) δ 173.6, 156.1, 138.4, 136.9, 132.4, 130.5, 129.4, 127.7, 123.8, 117.2, 65.7, 55.3, 39.4, 32.8, 30.6, 30.5, 30.5, 30.4, 30.2, 30.2, 29.5, 26.8, 25.7, 25.5, 25.3, 25.1, 23.6, 18.4, 15.0.

HRMS (ESI, m/z) 877.5807 [M + Na]$^+$, 877.5814 calculated for $C_{52}H_{78}N_4O_6Na$.

Chiral HPLC Chiralpak IA, heptane/ethanol 70/30, 1 ml/min, UV 230 nm: e.e.: >99.5 %, d.r.: >99.5:0.5.

B

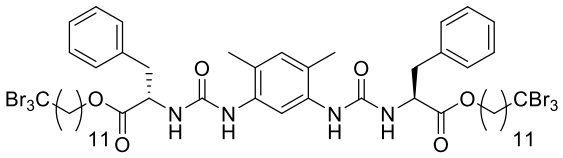

Preparation was achieved following method B using 12-tribromododecyl (*S*)-phenylalaninate ammonium tosylate salt (**6**). The crude mixture was recrystallized from acetonitrile yielding pure **B** (0.71 g, 28%) as a white paste.

^{1}H NMR (300 MHz, DMSO-d_6) δ 7.95 (s, 1H, Ar*H*), 7.75 (s, 2H, N*H*), 7.35-7.15 (m, 10H, Ar*H* and N*H*), 6.85 (s, 1H, Ar*H*), 6.70 (d, 2H, Ar*H*, J = 7.8 Hz), 4.49 (q, 2H, NH-C*H*, J = 7.2 Hz), 4.00 (t, 4H, COO-CH_2, J = 6.4 Hz), 3.05-2.90 (m, 8H, CBr_3-CH_2 and NH-CH-CH_2), 2.05 (s, 6H, Ar-CH_3), 1.67 (quint, 4H, COO-CH_2-CH_2, J = 7.3 Hz), 1.58-1.15 (m, 32H, CH_2).

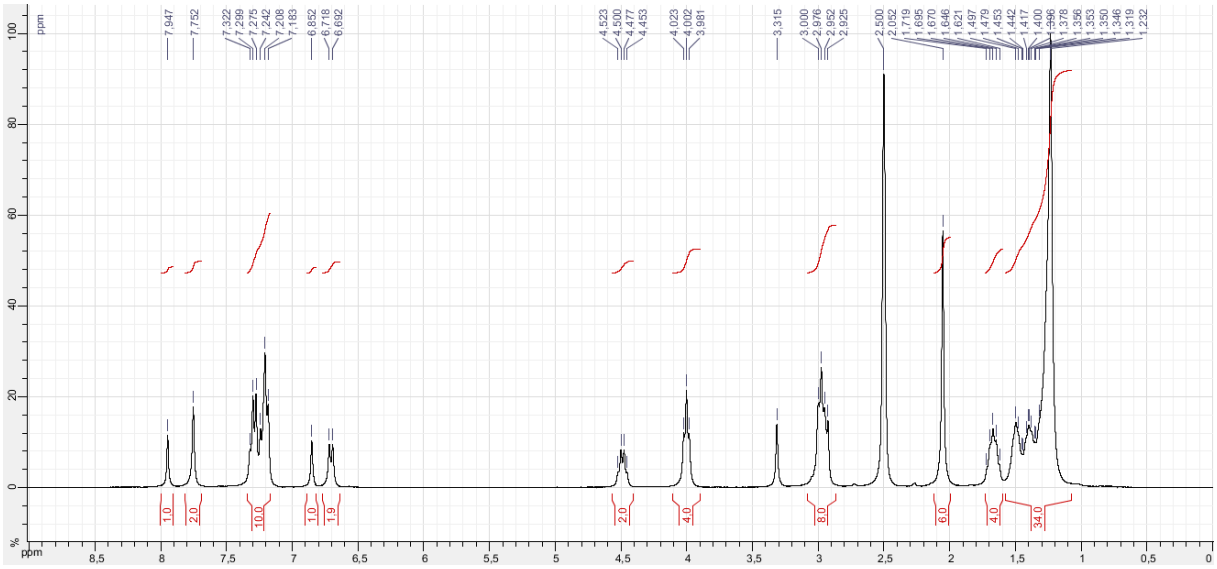

Figure S17. ^{1}H NMR of **B** (300 MHz in DMSO-d_6)

^{13}C{^{1}H} NMR (101 MHz, DMSO-d_6) δ 172.3, 154.7, 144.5, 137.6, 136.9, 135.3, 131.2, 129.1, 128.2, 126.5, 122.4, 64.4, 58.7, 53.9, 43.4, 37.7, 29.2, 28.8, 28.7, 28.6, 28.0, 27.1, 25.3, 17.2.

HRMS (ESI, m/z) 1349.0413 $[M + Na]^+$, 1349.0403 calculated for $C_{52}H_{72}Br_6N_4O_6Na$.

Chiral HPLC Lux-Cellulose-4, heptane/ethanol 70/30, 1 ml/min, UV 254 nm: e.e.: >99.5 %, d.r.: 99 :1.

C

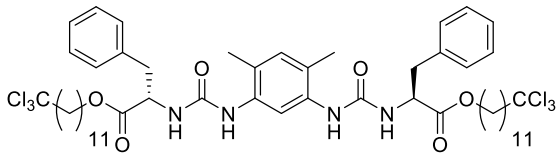

Preparation was achieved following method B using 12-trichlorododecyl (*S*)-phenylalaninate ammonium tosylate salt (**9**). The crude mixture was recrystallized from acetonitrile yielding pure **C** (0.29 g, 64%) as a white paste.

^{1}H NMR (300 MHz, DMSO-d_6) δ 7.95 (s, 1H, Ar*H*), 7.75 (s, 2H, N*H*), 7.35-7.15 (m, 10H, Ar*H* and N*H*), 6.85 (s, 1H, Ar*H*), 6.70 (d, 2H, Ar*H*, J = 7.8 Hz), 4.49 (q, 2H, NH-C*H*, J = 7.2 Hz), 4.00 (t, 4H, COO-CH_2, J = 6.4 Hz), 3.04-2.94 (m, 4H, NH-CH-CH_2), 2.72 (t, 4H, CCl_3-CH_2, J = 7.9 Hz), 2.05 (s, 6H, Ar-CH_3), 1.67 (quint, 4H, COO-CH_2-CH_2, J = 7.3 Hz), 1.58-1.15 (m, 32H, CH_2).

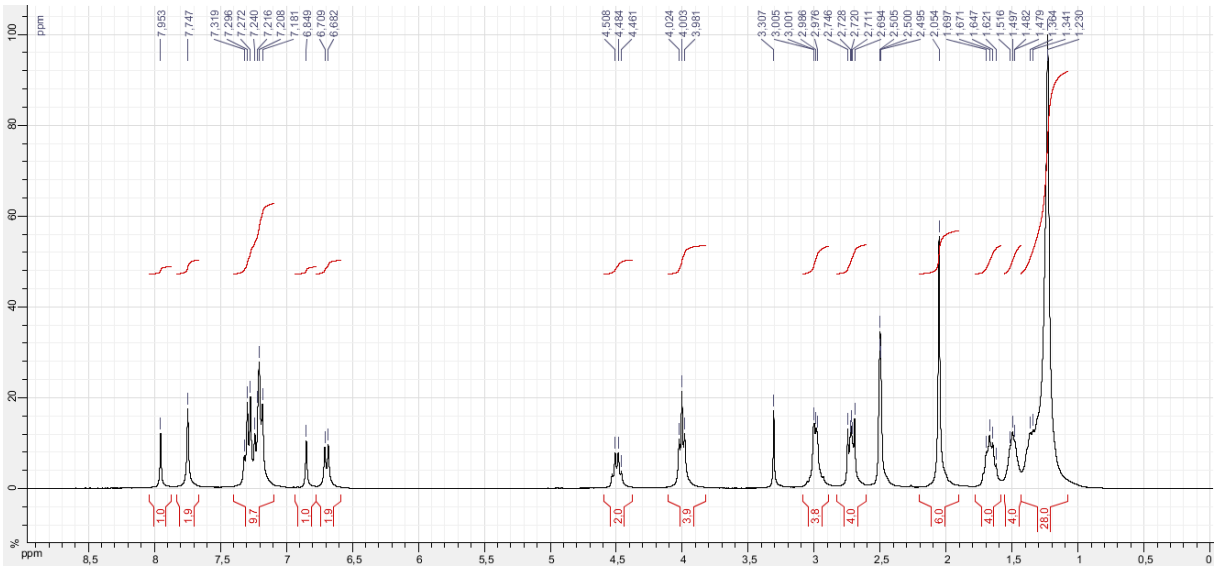

Figure S18. ^{1}H NMR of **C** (300 MHz in DMSO-d_6)

^{13}C{^{1}H} NMR (75 MHz, DMSO-d_6) δ 172.8, 155.2, 137.4, 135.8, 131.7, 129.6, 128.7, 127.0, 122.9, 116.2, 101.0, 64.9, 54.6, 54.4, 38.3, 29.3, 29.3, 29.2, 29.1, 28.5, 28.0, 26.6, 25.8, 17.7.

HRMS (ESI, m/z) 1083.3474 $[M + Na]^+$, 1083.3446 calculated for $C_{52}H_{72}Cl_6N_4O_6Na$.

References

(1) Lortie, F.; Boileau, S.; Bouteiller, L.; Chassenieux, C.; Deme, B.; Ducouret, G.; Jalabert, M.; Laupretre, F.; Terech, P. *Langmuir* **2002**, *18*, 7218.
(2) Dirany, M.; Ayzac, V.; Isare, B.; Raynal, M.; Bouteiller, L. *Langmuir* **2015**, *31*, 11443.
(3) Brocorens, P.; Linares, M.; Guyard-Duhayon, C.; Guillot, R.; Andrioletti, B.; Suhr, D.; Isare, B.; Lazzaroni, R.; Bouteiller, L. *J. Phys. Chem. B* **2013**, *117*, 5379.
(4) Mayo, S. L.; Olafson, B. D.; Goddard, W. A., III. *J. Phys. Chem.* **1990**, *94*, 8897.
(5) Kolar, M. H.; Hobza, P. *Chem. Rev.* **2016**, *116*, 5155.
(6) Sun, H. *J. Comput. Chem.* **1994**, *15*, 752.
(7) Sun, H. *Macromolecules* **1995**, *28*, 701.
(8) Nose, S. *Mol. Phys.* **1984**, *52*, 255.
(9) Verlet, L. *Phys. Rev.* **1967**, *159*, 98.
(10) Gaussian 09, Revision E.01, M. J. Frisch, G. W. Trucks, H. B. Schlegel, G. E. Scuseria, M. A. Robb, J. R. Cheeseman, G. Scalmani, V. Barone, B. Mennucci, G. A. Petersson, H. Nakatsuji, M. Caricato, X. Li, H. P. Hratchian, A. F. Izmaylov, J. Bloino, G. Zheng, J. L. Sonnenberg, M. Hada, M. Ehara, K. Toyota, R. Fukuda, J. Hasegawa, M. Ishida, T. Nakajima, Y. Honda, O. Kitao, H. Nakai, T. Vreven, J. A. Montgomery, Jr., J. E. Peralta, F. Ogliaro, M. Bearpark, J. J. Heyd, E. Brothers, K. N. Kudin, V. N. Staroverov, R. Kobayashi, J. Normand, K. Raghavachari, A. Rendell, J. C. Burant, S. S. Iyengar, J. Tomasi, M. Cossi, N. Rega, J. M. Millam, M. Klene, J. E. Knox, J. B. Cross, V. Bakken, C. Adamo, J. Jaramillo, R. Gomperts, R. E. Stratmann, O. Yazyev, A. J. Austin, R. Cammi, C. Pomelli, J. W. Ochterski, R. L. Martin, K. Morokuma, V. G. Zakrzewski, G. A. Voth, P. Salvador, J. J. Dannenberg, S. Dapprich, A. D. Daniels, Ö. Farkas, J. B. Foresman, J. V. Ortiz, J. Cioslowski, and D. J. Fox, Gaussian, Inc., Wallingford CT, 2009. .
(11) Finkelstein, H. *Berichte Dtsch. Chem. Ges.* **1910**, *43*, 1528.
(12) Gorske, B. C.; Mbofana, C. T.; Miller, S. J. *Org. Lett.* **2009**, *11*, 4318.
(13) Lee, E.; Park, C. M.; Yun, J. S. *J. Am. Chem. Soc.* **1995**, *117*, 8017.
(14) Cantekin, S.; ten Eikelder, H. M. M.; Markvoort, A. J.; Veld, M. A. J.; Korevaar, P. A.; Green, M. M.; Palmans, A. R. A.; Meijer, E. W. *Angew. Chem. Int. Ed.* **2012**, *51*, 6426.
(15) Giannicchi, I.; Jouvelet, B.; Isare, B.; Linares, M.; Dalla Cort, A.; Bouteiller, L. *Chem. Commun.* **2014**, *50*, 611.